ACCOUNTS
of chemical research

Heterogeneity in Polymer Solar Cells: Local Morphology and Performance in Organic Photovoltaics Studied with Scanning Probe Microscopy

CHRIS GROVES, OBADIAH G. REID, AND DAVID S. GINGER*

Department of Chemistry, University of Washington, Seattle, Washington 98195, USA

RECEIVED ON SEPTEMBER 1, 2009

CONSPECTUS

The use of organic photovoltaics (OPVs) could reduce production costs for solar cells because these materials are solution processable and can be manufactured by roll-to-roll printing. The nanoscale texture, or film morphology, of the donor/acceptor blends used in most OPVs is a critical variable that can dominate both the performance of new materials being optimized in the lab and efforts to move from laboratory-scale to factory-scale production. Although efficiencies of organic solar cells have improved significantly in recent years, progress in morphology optimization still occurs largely by trial and error, in part because much of our basic understanding of how nanoscale morphology affects the optoelectronic properties of these heterogeneous organic semiconductor films has to be inferred indirectly from macroscopic measurements.

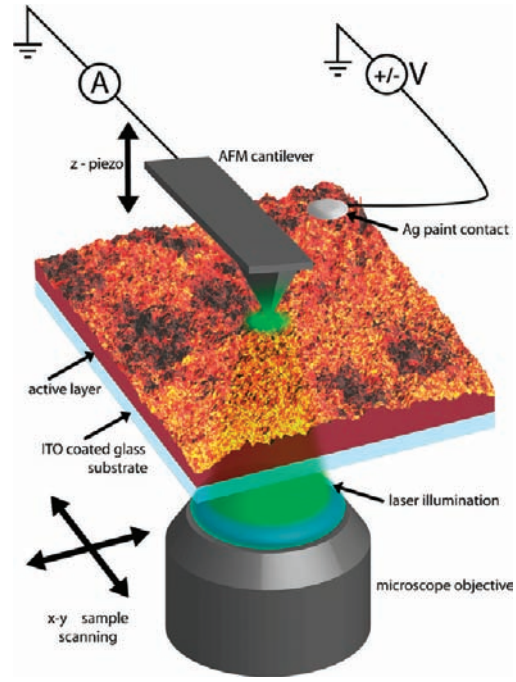

In this Account, we review the importance of nanoscale morphology in organic semiconductors and the use of electrical scanning probe microscopy techniques to directly probe the local optoelectronic properties of OPV devices. We have observed local heterogeneity of electronic properties and performance in a wide range of systems, including model polymer−fullerene blends such as poly(3-hexylthiophene) (P3HT) and [6,6]-phenyl-C_{61}-butyric acid methyl ester (PCBM), newer polyfluorene copolymer−PCBM blends, and even all polymer donor−acceptor blends. The observed heterogeneity in local photocurrent poses important questions, chiefly what information is contained and what is lost when using average values obtained from conventional measurements on macroscopic devices and bulk samples? We show that in many cases OPVs are best thought of as a collection of nanoscopic photodiodes connected in parallel, each with their own morphological and therefore electronic and optical properties. This local heterogeneity forces us to carefully consider the adequacy of describing OPVs solely by "average" properties such as the bulk carrier mobility. Characterizing this local heterogeneity in the morphology of an OPV and the consequent variations in local performance is vital to understanding OPV operation.

Introduction

OPVs can be made from a variety of solution-processable materials, but we will focus on OPVs fabricated from blends of either two conjugated polymers or a conjugated polymer and a fullerene derivative. Conjugated polymers are attractive solution-processable materials for optoelectronic applications because of the tunability of their opto-

Published on the Web 02/09/2010 www.pubs.acs.org/acr
10.1021/ar900231q

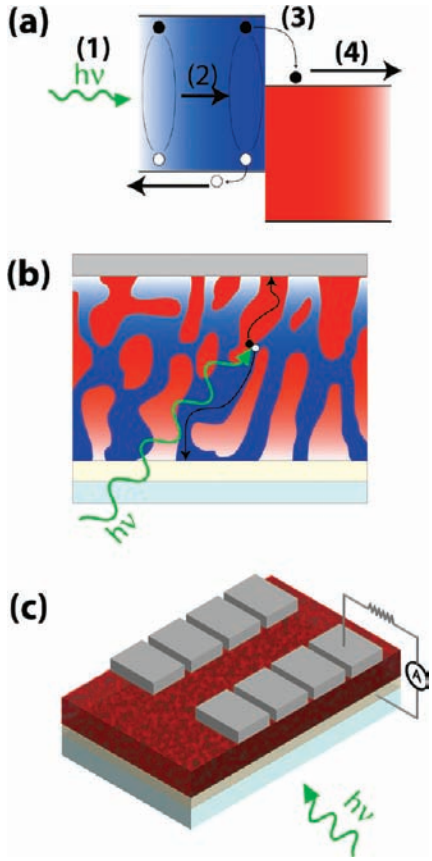

FIGURE 1. Schematic representations of (a) charge generation at a type II heterojunction, (b) charge transport through the bulk heterojunction to the collecting electrodes, and (c) the layer structure of a typical OPV device.

electronic properties afforded through control of their chemical structure. However, solar cells made from conjugated polymers function differently than devices made from inorganic semiconductors. One of the most important differences is that the absorption of photons in an organic semiconductor does not directly produce free charges. In an OPV, absorption of a photon leads to the formation of a neutral excited state called an exciton (consisting of a tightly bound electron−hole pair) that must be dissociated to yield the charge carriers needed for a photocurrent. Since the exciton binding energy (∼0.2−0.5 eV)[1,2] is much greater than the thermal energy (∼25 meV), exciton dissociation is commonly accomplished using two materials with energy levels that form a type-II heterojunction, shown schematically in Figure 1a. At a type-II interface, the exciton will be dissociated through the energetically favorable transfer of an electron to the electron acceptor (usually a fullerene derivative), or a hole to the electron donor (usually a conjugated polymer). The resulting electron and hole can then travel through the electron acceptor and electron donor networks to the electrodes, as shown schematically in Figure 1b.

The need for a heterojunction in an OPV presents a challenge since excitons typically diffuse only ∼10 nm in a conjugated polymer before relaxing,[3] while the optical absorption length of organic materials is typically ∼100 nm. Therefore, to achieve good absorption *and* good exciton dissociation efficiency, one must use an optically thick film in which the two components are mixed roughly on the scale of the exciton diffusion length as shown in Figure 1b. Such a structure is called a bulk heterojunction (BHJ) and can be produced by blending the two component materials in a common solution prior to deposition. The structure of a typical OPV device is shown in Figure 1c.

Exciton dissociation is not the only challenge we need to overcome to produce a useful photocurrent from an OPV. The geminate electron−hole pair formed when the exciton dissociates across the donor/acceptor interface feels a strong Coulombic attraction due to the low dielectric constant of organic semiconductors ($\varepsilon \approx 3$). Thus, even after charge transfer across the heterojunction, the electron and hole from the original exciton may remain bound and undergo geminate recombination. The degree of geminate recombination is determined by the competition of the recombination processes[4] with the charge transport processes that lead to free charges. There is a growing body of evidence that geminate recombination can be a significant loss mechanism for solution-processable OPVs.[5−7] Geminate recombination is dependent upon the external field[8] and, of particular importance here, is also dependent upon the BHJ morphology, both directly through the size of the domains and the orientation of the heterointerfaces with respect to the field[8] and indirectly through the morphology dependence of mobility[9] and interfacial states.[10] Geminate pair separation[8] is favored by larger domains, counter to the preference for finer domains needed to maximize exciton dissociation.

Subsequent charge transport is also highly sensitive to film morphology. The alignment and connectivity of the domains clearly affect the ability of charges to reach the electrodes. In addition, the materials that form the blend exist in a variety of conformations, packings, and local environments, and as a result the carriers experience a disordered energetic landscape. Energetic disorder divides up the OPV into areas where it is more or less favorable for a charge to travel within the donor or acceptor. Hence, a consequence of energetic disorder is likely to be filamentary transport, that is, the preferential flowing of carriers through low-energy routes through the film.[11,12]

The morphology of the BHJ affects nearly all aspects of OPV performance including charge generation, charge sepa-

ration, and charge transport. This is problematic, since morphology is itself a complex phenomenon and can be challenging to predict or control experimentally. The typical BHJ morphology is essentially a metastable state that is frozen in at the end of the drying process, although further morphology evolution can be provided by thermal or solvent-vapor annealing.[13−18] Additional factors that can exert an influence on the morphology include molecular weight of the polymer,[19] polymer regioregularity,[20] solvent,[21] side-chain length,[22] and weight percentage of the polymers.[23] Surface chemistry can also lead to wetting of a component at the air or substrate interface.[24] Patterned surface chemistry can even be used to direct lateral as well as vertical composition gradients.[25] Because the BHJ morphology is sensitive to so many parameters, the details of the morphology, such as domain size and packing, are not always uniform throughout the film. Heterogeneities in the BHJ morphology are common in polymer/polymer[26−28] and polymer/fullerene[13,18,29] films.

The connection between morphology and OPV performance has motivated a large number of studies. To date, an impressive array of tools has been applied to characterize organic semiconductor film morphology. These techniques range from routine X-ray diffraction,[16] electron microscopy,[23,30] and atomic force microscopy (AFM)[23] to more advanced 3D electron tomography[31,32] and even synchrotron-based structural studies.[33,34] However, while these tools provide valuable structural data, they do not provide direct correlations between the local structure (length scale, composition, and connectivity of domains) and local electronic properties (photocurrent, carrier mobility, trap density). Instead, these tools are limited to inferring how *average* features of the morphology affect the performance of macroscopic devices. Hence there is a risk that any links between *local* variations in morphology and consequent *local* variations in device performance can be lost, since the morphology is rarely uniform throughout the film. What is needed, both for improving our fundamental understanding of nanostructured organic solar cells and for advancing manufacturing and materials development, are techniques capable of mapping local photocurrents and deconvoluting the varying local contributions of charge generation, recombination, and transport to overall device performance. In this Account, we highlight how electrical scanning probe microscopy techniques can be used to provide just this sort of critical detail to link *local* variations in morphology with *local* variations in OPV performance.

Experimental Details: Photoconductive AFM and Time-Resolved Electrostatic Force Microscopy

Scanning probe microscopy is an ideal tool for studying OPV materials that are heterogeneous on 10−100 nm length scales because it has high resolution and a variety of image formation mechanisms. Groups have used a wide variety of variations to study the local optoelectronic properties of OPVs including conductive AFM (cAFM),[35] near-field scanning optical microscopy,[27,36] scanning Kelvin probe microscopy,[37,38] and electrostatic force microscopy.[38] We review two such methods, the first being conductive and photoconductive AFM (pcAFM) and the second being time-resolved electrostatic force microscopy (trEFM).

The apparatus and experimental technique used for cAFM and pcAFM measurements in our laboratories are depicted schematically in Figure 2a and described in detail elsewhere.[38,39] In cAFM and pcAFM, a metal-coated cantilever with a soft spring constant is used to image in contact mode and also to form the top electrical contact to the polymer film.[40] For cAFM, a bias is applied in the dark and the resulting injection current is measured. This technique is useful for a number of applications, such as making local space-charge-limited mobility measurements[39] and mapping local variations in chemical composition using the contrast provided by differing carrier mobilities or injection barriers.[25] pcAFM is similar to cAFM but with the addition of a diffraction-limited laser spot to illuminate the OPV material directly beneath the AFM tip. With no external bias, pcAFM can yield maps of local short-circuit photocurrent that are correlated with local topography at a resolution limited by the AFM tip (∼15 nm). In addition, local $I-V$ characteristics including fill factor and open-circuit voltage can be obtained at specific points on the film. Note that spatially averaged photocurrent[40] and mobility[39] measurements taken by pcAFM and cAFM agree well with measurements made on bulk devices with evaporated contacts.

In trEFM, an AC-mode conductive cantilever with a stiffer spring constant is used ($k \approx 20$ N/m, $\omega \approx 70-350$ kHz), but in this case, the cantilever is raised a small distance above the surface of the sample and mechanically driven at its resonant frequency. The tip and sample form a capacitor, and the electrostatic force gradient on the tip causes a shift in the cantilever resonance frequency when a bias is applied. When the OPV material is excited optically, carriers are formed. These charges alter the local electrostatic force gradient between the tip and the sample and thus create a new shift in the reso-

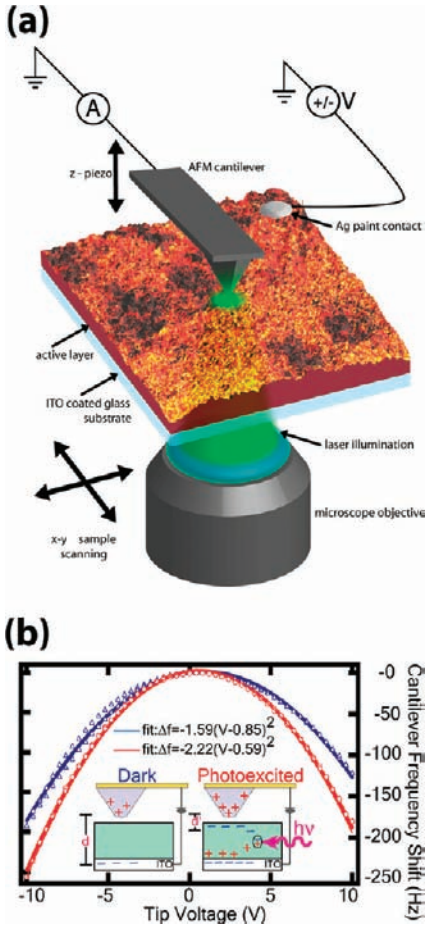

FIGURE 2. (a) Schematic diagram of the pcAFM (trEFM) measurement system: a conducting AFM tip is coaligned with a laser (or pulsed LED) to provide simultaneous electrical bias and optical excitation to a specific area of the sample. (b) Cantilever shift frequency versus tip bias in a trEFM measurement for a PFB/F8BT blend film in the dark (blue triangles) and under illumination (red circles); inset shows schematically the difference in charge distribution for the two cases, which leads to the measured electrostatic force gradient.

nance frequency. By recording how fast the resonance frequency shifts following photoexcitation at each position, trEFM can thus be used to map local photogeneration activity. Figure 2b shows the mechanism of trEFM image formation. We have found empirically that the rate of change in this resonance frequency following optical excitation of the sample is directly proportional to the short circuit photocurrent in macroscopic photodiodes.[26]

Imaging Currents and Photocurrents in Polymer Solar Cells

We have used pcAFM and trEFM to correlate charge transport and local photocurrent generation with morphology in a range of archetypal donor/acceptor blends. Consistent with the expectations outlined in the introduction section, we have observed significant heterogeneity in the electrical properties in many systems.

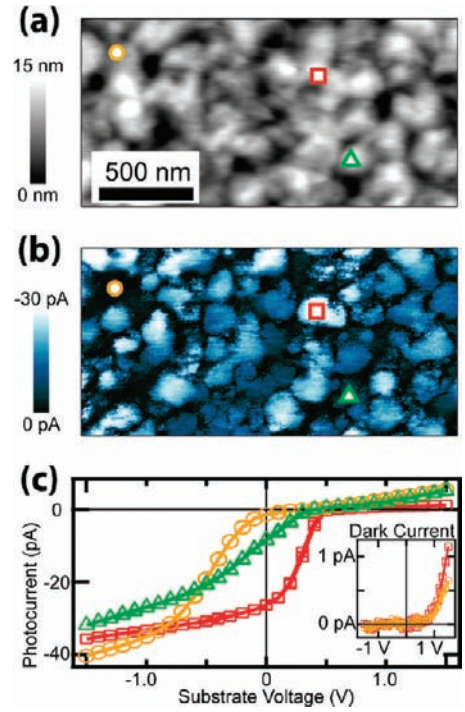

FIGURE 3. (a) AFM height image of an MDMO-PPV/PCBM (20:80 ratio) film spin-coated from xylene, (b) photocurrent map measured with zero external bias and an illumination intensity of 10^4 W m^{-2} at 532 nm and (c) local current−voltage data acquired at the three locations indicated by the symbols in panels a and b. Inset shows local current−voltage data without illumination showing smaller dark currents.

Nanoscale and Microscale Heterogeneity in Alkoxy-PPV Blends. Conjugated polymers based on derivatives of poly(phenylene vinylene) (PPV) were among the first to be used in OPVs,[41,42] though the power conversion efficiency was low (<1%). Later, Shaheen et al. found that by changing the solvent to chlorobenzene, the power conversion efficiency of poly(2-methoxy-5-(3′,7′-dimethyloctyl-oxy)-1,4-phenylene vinylene) (MDMO-PPV or OC1C10-PPV)/[6,6]-phenyl-C_{61}-butyric acid methyl ester (PCBM) solar cells was improved to 2.5%.[43] This observation launched a new wave of interest in OPVs, while at the same time underscoring the important role that processing conditions and film morphology can have on device performance.

We applied pcAFM to examine local photocurrent collection in MDMO-PPV/PCBM blends, and observed significant heterogeneity in the photocurrents of blends processed from different solvents.[40] Figures 3a,b,c, respectively show the topography, spatially resolved photocurrent generated by a 532 nm laser, and corresponding *J*−*V* curves under illumination recorded at various points on the surface of a film spin-coated from xylene (the positions of which are indicated by

the symbols in Figure 3a,b) as measured by pcAFM. The processing conditions yielded a surface topography with feature sizes of ~100 nm and surface roughness of ~15 nm. These topographical features are due to ~20−100 nm PCBM crystallites suspended within the blend matrix, as has been shown by cross-sectional SEM on similar devices.[30] Figure 3b shows the photocurrent collected with the cAFM tip at zero bias on the same area of the sample shown in Figure 3a. Significantly, the photocurrent varies by more than an order of magnitude over the area examined. Additionally, the photocurrent shows features of ~20−100 nm in size within which the photocurrent is largely uniform. While the photocurrent features are associated with the PCBM crystallites, not all crystallites affect the current in the same way. For example, the square and the triangle in Figure 3a,b mark two topographically similar points on the film; however, the photocurrent varies by a factor of 3. We attribute this variation to differences in vertical morphology, as suggested by the cross-sectional SEM images of Hoppe et al.,[30] indicating that the vertical position of the PCBM crystallites can play a critical role in determining local performance in addition to lateral morphology. The local variations in short-circuit current are correlated with variations in the local $J-V$ curves shown in Figure 3c, with open-circuit voltages varying from 0.35 to 0.53 V and fill factors varying from 0.42 to 0.58. Similar variations were present even when the films were processed from the "optimal" chlorobenzene solvent. Clearly, the local heterogeneity in the film morphology causes significant local variations in performance.

These findings suggested that we should think of a BHJ device as being composed of many nanoscale devices wired in parallel. Each of these nanoscale devices possesses distinct morphological and hence electronic properties. Consequently, the macroscopic device performance is limited by the presence of the poorly performing domains (i.e., those with lower open-circuit voltages and short-circuit currents). These data show that improvements in performance are still possible provided one can reduce the proportion of unproductive areas within the film, highlighting the important role scanning probe microscopy techniques could play in optimizing the performance of new materials for OPVs.

Evolution of Heterogeneity upon Annealing Polythiophene/Fullerene Blends. Although PPV derivatives still remain an important model system for OPVs, they have been eclipsed in importance over the past few years by blends of polythiophene donors with fullerene acceptors. Exhibiting good hole mobility and absorption out to ~630 nm and having been widely available from commercial sources for a number of years, regioregular poly(3-hexylthiophene) (P3HT) is

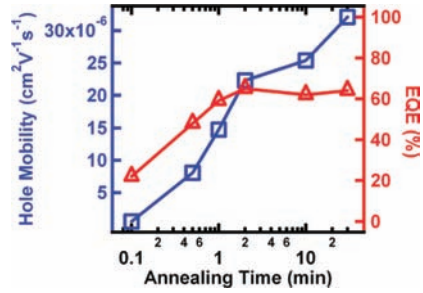

FIGURE 4. Bulk hole mobility (blue squares) and device external quantum efficiency (red triangles) as a function of annealing time for P3HT/PCBM solar cells.

perhaps the best-studied donor polymer at the time of writing. Although P3HT/PCBM blends have been surpassed in OPV performance by a number of other donor/acceptor combinations,[44] P3HT/PCBM remains an important model system, both because of the wealth of structural and performance data available to test models of device efficiency and because many new materials under development share structural or morphological similarities (or both) with P3HT.

Optimization of film morphology is critical to obtaining good performance from P3HT/PCBM blends. Typically, a ~1:1 by weight blend of P3HT/PCBM is deposited from a chlorobenzene solution.[45] If devices are fabricated from an "as cast" P3HT/PCBM film, one obtains power conversion efficiencies in the range of 1%, open-circuit voltages of ~0.6 V, short-circuit currents of ~4 mA/cm^2, and fill factors of ~35%.[45] However, the overall device performance can be improved considerably if the P3HT/PCBM film is treated to allow the morphology to coarsen. This is most commonly done either by annealing the films at elevated temperature[13,15,17,45] or in an atmosphere of solvent vapor.[16] The large improvement in performance gained by annealing in P3HT/PCBM solar cells has been attributed to improved hole mobility[9] as well as an increase in optical density and red-shifted absorption.[46,47] Both effects are associated with crystallization of the P3HT into lamellar structures and the orientation of the lamella. It is the consensus expectation that the improved hole mobility is particularly important because it will lead to more balanced transport.[9] However, upon annealing the blend morphology becomes increasingly coarse and heterogeneous.[13,17] Therefore, we find it important to ask whether the improvement in performance that occurs during annealing of P3HT/PCBM devices is best described in terms of average bulk characteristics such as hole mobility or whether a more local description that includes heterogeneity of the morphology is important.

Figure 4 shows the bulk external quantum efficiency (EQE) and bulk hole mobility measured on space-charge-limited

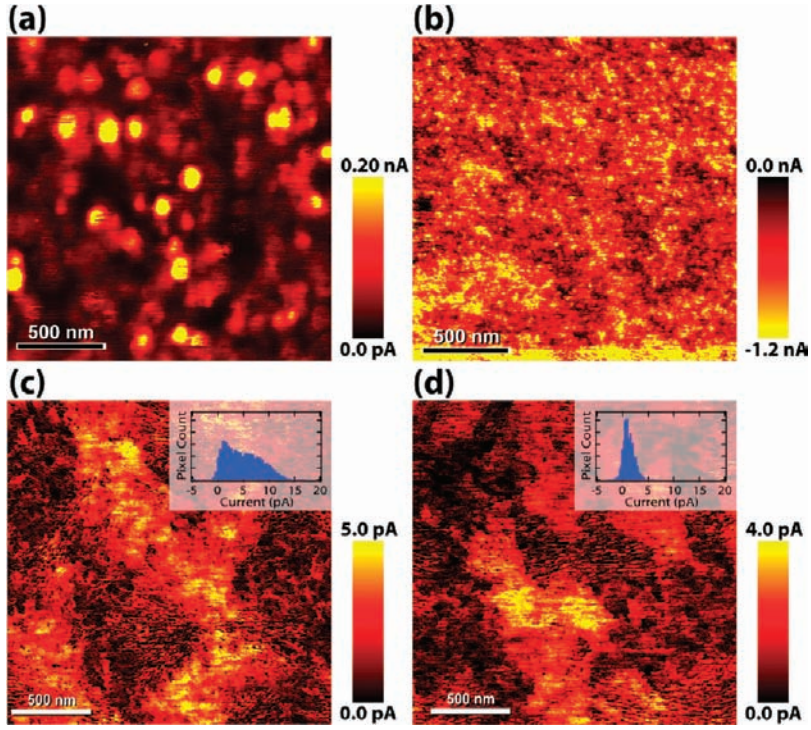

FIGURE 5. Images a, b, and c taken on a P3HT/PCBM solar cell after 2 min of annealing and (d) an unannealed device: (a) electron-dominated dark current (collected at −5 V tip bias), (b) hole-dominated dark current (collected at +5 V tip bias), and (c, d) short-circuit photocurrent for the devices annealed at 2 and 0 min when excited with 532 nm laser light. Insets to panels c and d show corresponding photocurrent histograms.

diodes as a function of annealing time. Similar to other studies,[13,17] we observed that the EQE and power conversion efficiency improve significantly with annealing. The power conversion efficiency of our devices is shown to plateau after ∼2 min. In contrast, we found that the hole mobility continued to increase by up to 45% over much longer annealing times (up to 30 min) after the EQE has saturated. We note that some annealing protocols produce P3HT/PCBM devices in which the hole mobility and the device performance are well correlated.[9] These differences underscore the fact that OPV performance can be sensitive to small variations in processing conditions. Nevertheless, our data show that bulk measurements and average parameters cannot always explain the processes determining device performance. To investigate the annealing process at the local level, we performed pcAFM and cAFM measurements on P3HT/PCBM devices after different annealing times.[29]

Figure 5a,b,c shows the electron-dominated dark current (collected at −5 V tip bias), hole-dominated dark current (collected at +5 V tip bias), and short-circuit photocurrent, respectively, measured on the same area of a P3HT/PCBM device that was annealed for 2 min. Figure 5d shows the short-circuit photocurrent for an unannealed device. It can be seen that increased annealing leads to increased heterogeneity, a trend that continues for all annealing times examined. The amount of dark current collected is affected by injection efficiency as well as transport through the film. Nevertheless, the dark current maps tend to reflect the position of the high-mobility routes through the blend film, and local average currents measured with cAFM tend to be proportional to the average mobility measured on macroscopic space-charge-limited diodes measured on the same films.[39] What is striking when comparing Figure 5a−c is the apparent lack of correlation, and even anticorrelation, between areas of electron dark current, hole dark current, and photocurrent. An annotated version of the photocurrent image, which highlights this anticorrelation, is available in ref 29. Anticorrelation between the electron and hole dark currents is indicative of compositional variations across the film. A local improvement in transport for one carrier should come at the cost of poor transport for the other, since the minority component of the blend forms a poor percolating network between the electrodes.[48] Why photocurrent and dark current should be anticorrelated is, however, less obvious. One might expect that improved charge transport would improve geminate dissociation efficiency and therefore photocurrent.[8] To understand these data, we must also consider exciton dissociation efficiency. If we consider an area rich in P3HT, the hole transport may be optimized, how-

ever, the heterojunction surface area immediately available for exciton dissociation could be reduced due to the smaller amount of PCBM. Therefore, the areas of highest dark current could be excluded from also being areas of highest photocurrent. For optimal photocurrent, we instead wish to strike a balance in the morphology between exciton dissociation and subsequent geminate separation efficiency.[49]

Our data show that the areas of the device that contribute significantly to the dark current are not always the same as those that contribute significantly to the photocurrent. Hence, a film with the highest bulk hole mobility (related to dark current) will not always produce the highest EQE (related to photocurrent). Taken to the extreme, this conclusion is apparent: a film comprising millimeter-sized domains of pure crystallized P3HT and PCBM would show optimal bulk mobilities due to the continuous charge transport pathways but poor photocurrent due to the minimal interfacial area. However, the details in real devices are more complicated. For instance, the formation of large (10−100 μm) PCBM crystallites can sometimes be associated with increased performance during solvent-vapor annealing of polyfluorene copolymer based solar cells.[18] Using local imaging, we showed that the large crystallites themselves were not associated with increased performance; rather they acted as sinks for excess PCBM, thereby allowing the neighboring film regions to adopt more a optimal nanoscale morphology.[18]

The Role of Nanostructured Interfaces in All-Polymer OPVs. Another approach to tailor the performance OPVs is to replace the fullerene with a polymer, perhaps one that absorbs more light or that offers more scope for tailoring HOMO and LUMO levels than a fullerene. Blends of poly-(9,9′-dioctylfluorene-*co*-benzothiadiazole) (F8BT) and poly(9,9′-dioctylfluorene-*co*-bis-*N*,*N*′-(4,butylphenyl)-bis-*N*,*N*′-phenyl-1,4-phenylenediamine) (PFB) are perhaps the all-polymer equivalent of P3HT/PCBM blends because their performance is not optimal but they represent a well-studied model system for understanding the effects of morphology on device performance and are thus an attractive system for scanning probe studies. In particular, PFB/F8BT films deposited from xylene solutions are attractive for studying the effects of morphology on OPV performance as the high boiling-point solvent leads to ∼100−1000 nm sized domains that are readily visible with atomic force microscopy[14] as shown in Figure 6a.[26] However, some studies have found that the performance of PFB/F8BT OPVs scales with the visible interface area between domains over certain compositions,[28] whereas others suggest that the majority of the photocurrent is produced from the centers of the domains and not at the interfaces.[27]

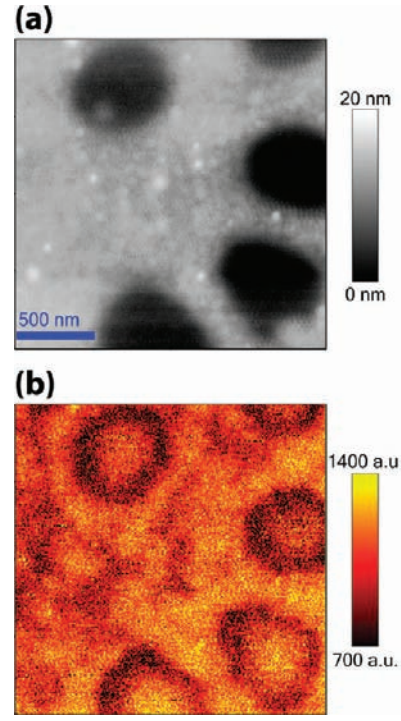

FIGURE 6. (a) AC-mode AFM topography image of a 50:50 film of PFB/F8BT spin coated from xylene, the recessed domains being PFB-rich, and (b) trEFM photoinduced charging rate map, generated by plotting the inverse exponential time constant for photoinduced charging at each point on the same area as shown in panel a. Note that the dark rings indicate areas of slower charging/lower performance.

We used trEFM to measure both the morphology of PFB/F8BT blends and the photoinduced charging rate.[26] Figure 6b shows the trEFM charging rate from the same area as the topography image of Figure 6a. Surprisingly, the areas with the highest charging rates are at the centers of the topographically visible domains, not their edges. Indeed, the edges of the domain show reduced photocurrent. This suggests that the visible domain edges likely act as recombination centers, (a hypothesis consistent with a number of other imaging and spectroscopic studies on PFB/F8BT blends).[27,50] Increased recombination at the visible domain boundaries may be due to local composition or chain orientation at the domain boundaries. This result is in direct contradiction to a simple interpretation of the AFM topography images and once again emphasizes the importance of correlating local electronic and structural measurements.

Outlook

The observed heterogeneity in local photocurrent poses the important question as to what information is contained and what is lost when using average values obtained from conventional measurements on macroscopic devices and bulk

samples. We conclude that in many cases OPVs are best thought of as a collection of nanoscopic photodiodes connected in parallel, each with their own morphological and therefore electronic and optical properties. Furthermore, we have seen that regions of high dark current and high photocurrent are not always coincident. The implication is that different bulk measurements (for example, mobility and short-circuit current) may probe different subnetworks within a device, making the understanding of OPV performance solely in terms of bulk measurements challenging. In order to understand OPVs better we need to move beyond viewing the BHJ as a homogeneous medium with average properties.

Fortunately, several groups have been developing models that can consider the full 3D morphology of an OPV. For instance, using Monte Carlo models, it has been possible to study the effect of morphology upon efficiency,[8,49] open-circuit voltage, and short-circuit current.[49,51] We anticipate that these modeling techniques are likely to be useful in the interpretation of the data collected by the scanning probe techniques examined here. In particular, Monte Carlo models allow separate examination of charge generation, recombination, and transport that collectively result in the current measured by scanning-probe microscopy. In the near term, we think it should be particularly interesting to see whether experiments can resolve the anticipated presence of current filaments.[11,12] Direct measurements of current filaments and local current distributions would allow microscopic test of carrier transport physics in Monte Carlo or similar nanoscale models[11,52] and so help calibrate fully-3D models of OPV operation. Ultimately, models that allow for true morphology optimization as a function of local parameters are needed.

As both theory and experiment are refined, electrical scanning probe microscopy techniques will play an increasingly important role in both the microscopic understanding and technological optimization of OPVs. They can help us understand the microscopic effects of disorder on transport and mobility, as well as permit improved screening of new materials combinations by measuring local performance variations under different processing conditions. More broadly, local heterogeneity is not unique to OPVs, and we anticipate that as society's demand for new energy solutions increases, scanning probe methods will find new uses in studying new hybrid solar cell materials, mesostructured catalysts for photochemical fuel generation, and a range of other applications in energy conversion and light harvesting.

The authors acknowledge Kevin Noone for assistance preparing figures and acknowledge the NSF (Grants DMR-0120967 and DMR-0449422), AFOSR, DOE, and ONR for supporting different portions of the long-term research program described herein. D.S.G. also thanks the Camille Dreyfus Teacher-Scholar Awards program and the Alfred P. Sloan foundation for support.

BIOGRAPHICAL INFORMATION

Chris Groves graduated from Sheffield University (U.K.) with B.Eng. and Ph.D. degrees in 2001 and 2004, respectively. He has since worked as a postdoctoral researcher at the University of Cambridge (U.K.) and the University of Washington, before taking up his current post as Lecturer in Durham University (U.K.).

Obadiah G. Reid graduated from Pacific University in 2004 with a B.S. in Chemistry. After a year working at Pacific Northwest National Laboratory, he came to the University of Washington in 2005 and is presently a Ph.D. Candidate in the Department of Chemistry.

David S. Ginger earned dual B.S. degrees in chemistry and physics from Indiana University in 1997 and a Ph.D. in physics from the University of Cambridge (U.K.) in 2001. After a postdoctoral fellowship at Northwestern University, he joined the University of Washington in 2003, where he is currently an Associate Professor of Chemistry.

FOOTNOTES

*E-mail: ginger@chem.washington.edu.

REFERENCES

1 Bredas, J. L.; Cornil, J.; Heeger, A. J. The exciton binding energy in luminescent conjugated polymers. *Adv. Mater.* **1996**, *8*, 447–452.

2 Alvarado, S. F.; Seidler, P. F.; Lidzey, D. G.; Bradley, D. D. C. Direct determination of the exciton binding energy of conjugated polymers using a scanning tunneling microscope. *Phys. Rev. Lett.* **1998**, *81*, 1082–1085.

3 Scully, S. R.; McGehee, M. D. Effects of optical interference and energy transfer on exciton diffusion length measurements in organic semiconductors. *J. Appl. Phys.* **2006**, *100*, 034907.

4 Westenhoff, S.; Howard, I. A.; Hodgkiss, J. M.; Kirov, K. R.; Bronstein, H. A.; Williams, C. K.; Greenham, N. C.; Friend, R. H. Charge recombination in organic photovoltaic devices with high open-circuit voltages. *J. Am. Chem. Soc.* **2008**, *130*, 13653–13658.

5 Yin, C.; Kietzke, T.; Neher, D.; Horhold, H. H. Photovoltaic properties and exciplex emission of polyphenylenevinylene-based blend solar cells. *Appl. Phys. Lett.* **2007**, *90*, 092117.

6 McNeill, C. R.; Westenhoff, S.; Groves, C.; Friend, R. H.; Greenham, N. C. Influence of nanoscale phase separation on the charge generation dynamics and photovoltaic performance of conjugated polymer blends: Balancing charge generation and separation. *J. Phys. Chem. C* **2007**, *111*, 19153–19160.

7 Mihailetchi, V. D.; Koster, L. J. A.; Hummelen, J. C.; Blom, P. W. M. Photocurrent generation in polymer-fullerene bulk heterojunctions. *Phys. Rev. Lett.* **2004**, *93*, 216601.

8 Groves, C.; Marsh, R. A.; Greenham, N. C. Monte Carlo modeling of geminate recombination in polymer-polymer photovoltaic devices. *J. Chem. Phys.* **2008**, *129*, 114903.

9 Mihailetchi, V. D.; Xie, H. X.; de Boer, B.; Koster, L. J. A.; Blom, P. W. M. Charge transport and photocurrent generation in poly(3-hexylthiophene): methanofullerene bulk-heterojunction solar cells. *Adv. Funct. Mater.* **2006**, *16*, 699–708.

10 Huang, Y. S.; Westenhoff, S.; Avilov, I.; Sreearunothai, P.; Hodgkiss, J. M.; Deleener, C.; Friend, R. H.; Beljonne, D. Electronic structures of interfacial states formed at polymeric semiconductor heterojunctions. *Nat. Mater.* **2008**, *7*, 483–489.

11 van der Holst, J. J. M.; Uijttewaal, M. A.; Ramachandhran, B.; Coehoorn, R.; Bobbert, P. A.; de Wijs, G. A.; de Groot, R. A. Modeling and analysis of the three-dimensional current density in sandwich-type single-carrier devices of disordered organic semiconductors. *Phys. Rev. B* **2009**, *79*, 085203.

12 Kwiatkowski, J. J.; Nelson, J.; Li, H.; Bredas, J. L.; Wenzel, W.; Lennartz, C. Simulating charge transport in tris(8-hydroxyquinoline) aluminium (Alq3). *Phys. Chem. Chem. Phys.* **2008**, *10*, 1852–1858.

13 Yang, X. N.; Loos, J.; Veenstra, S. C.; Verhees, W. J. H.; Wienk, M. M.; Kroon, J. M.; Michels, M. A. J.; Janssen, R. A. J. Nanoscale morphology of high-performance polymer solar cells. *Nano Lett.* **2005**, *5*, 579–583.

14 Halls, J. J. M.; Arias, A. C.; MacKenzie, J. D.; Wu, W. S.; Inbasekaran, M.; Woo, E. P.; Friend, R. H. Photodiodes based on polyfluorene composites: Influence of morphology. *Adv. Mater.* **2000**, *12*, 498–502.

15 Padinger, F.; Rittberger, R. S.; Sariciftci, N. S. Effects of postproduction treatment on plastic solar cells. *Adv. Funct. Mater.* **2003**, *13*, 85–88.

16 Li, G.; Yao, Y.; Yang, H.; Shrotriya, V.; Yang, G.; Yang, Y. "Solvent annealing" effect in polymer solar cells based on poly(3-hexylthiophene) and methanofullerenes. *Adv. Funct. Mater.* **2007**, *17*, 1636–1644.

17 Ma, W. L.; Yang, C. Y.; Gong, X.; Lee, K.; Heeger, A. J. Thermally stable, efficient polymer solar cells with nanoscale control of the interpenetrating network morphology. *Adv. Funct. Mater.* **2005**, *15*, 1617–1622.

18 Bull, T. A.; Pingree, L. S. C.; Jenekhe, S. A.; Ginger, D. S.; Luscombe, C. K. The role of mesoscopic PCBM crystallites in solvent vapor annealed copolymer solar cells. *ACS Nano* **2009**, *3*, 627–636.

19 Schilinsky, P.; Asawapirom, U.; Scherf, U.; Biele, M.; Brabec, C. J. Influence of the molecular weight of poly(3-hexylthiophene) on the performance of bulk heterojunction solar cells. *Chem. Mater.* **2005**, *17*, 2175–2180.

20 Kim, Y.; Cook, S.; Tuladhar, S. M.; Choulis, S. A.; Nelson, J.; Durrant, J. R.; Bradley, D. D. C.; Giles, M.; McCulloch, I.; Ha, C. S.; Ree, M. A strong regioregularity effect in self-organizing conjugated polymer films and high-efficiency polythiophene: Fullerene solar cells. *Nat. Mater.* **2006**, *5*, 197–203.

21 Arias, A. C.; MacKenzie, J. D.; Stevenson, R.; Halls, J. J. M.; Inbasekaran, M.; Woo, E. P.; Richards, D.; Friend, R. H. Photovoltaic performance and morphology of polyfluorene blends: A combined microscopic and photovoltaic investigation. *Macromolecules* **2001**, *34*, 6005–6013.

22 Nguyen, L. H.; Hoppe, H.; Erb, T.; Gunes, S.; Gobsch, G.; Sariciftci, N. S. Effects of annealing on the nanomorphology and performance of poly(alkylthiophene): Fullerene bulk-heterojunction solar cells. *Adv. Funct. Mater.* **2007**, *17*, 1071–1078.

23 van Duren, J. K. J.; Yang, X. N.; Loos, J.; Bulle-Lieuwma, C. W. T.; Sieval, A. B.; Hummelen, J. C.; Janssen, R. A. J. Relating the morphology of poly(p-phenylene vinylene)/methanofullerene blends to solar-cell performance. *Adv. Funct. Mater.* **2004**, *14*, 425–434.

24 Germack, D. S.; Chan, C. K.; Hamadani, B. H.; Richter, L. J.; Fischer, D. A.; Gundlach, D. J.; DeLongchamp, D. M. Substrate-dependent interface composition and charge transport in films for organic photovoltaics. *Appl. Phys. Lett.* **2009**, *94*, 233303.

25 Coffey, D. C.; Ginger, D. S. Patterning phase separation in polymer films with dip-pen nanolithography. *J. Am. Chem. Soc.* **2005**, *127*, 4564–4565.

26 Coffey, D. C.; Ginger, D. S. Time-resolved electrostatic force microscopy of polymer solar cells. *Nat. Mater.* **2006**, *5*, 735–740.

27 McNeill, C. R.; Frohne, H.; Holdsworth, J. L.; Dastoor, P. C. Near-field scanning photocurrent measurements of polyfluorene blend devices: Directly correlating morphology with current generation. *Nano Lett.* **2004**, *4*, 2503–2507.

28 Snaith, H. J.; Arias, A. C.; Morteani, A. C.; Silva, C.; Friend, R. H. Charge generation kinetics and transport mechanisms in blended polyfluorene photovoltaic devices. *Nano Lett.* **2002**, *2*, 1353–1357.

29 Pingree, L. S. C.; Reid, O. G.; Ginger, D. S. Imaging the evolution of nanoscale photocurrent collection and transport networks during annealing of polythiophene/fullerene solar cells. *Nano Lett.* **2009**, *9*, 2946–2952.

30 Hoppe, H.; Niggemann, M.; Winder, C.; Kraut, J.; Hiesgen, R.; Hinsch, A.; Meissner, D.; Sariciftci, N. S. Nanoscale morphology of conjugated polymer/fullerene-based bulk-heterojunction solar cells. *Adv. Funct. Mater.* **2004**, *14*, 1005–1011.

31 Andersson, B. V.; Herland, A.; Masich, S.; Inganas, O. Imaging of the 3D nanostructure of a polymer solar cell by electron tomography. *Nano Lett.* **2009**, *9*, 853–855.

32 van Bavel, S. S.; Sourty, E.; de With, G.; Loos, J. Three-dimensional nanoscale organization of bulk heterojunction polymer solar cells. *Nano Lett.* **2009**, *9*, 507–513.

33 Kline, R. J.; McGehee, M. D.; Kadnikova, E. N.; Liu, J. S.; Frechet, J. M. J. Controlling the field-effect mobility of regioregular polythiophene by changing the molecular weight. *Adv. Mater.* **2003**, *15*, 1519–1522.

34 Toney, M. F.; Russell, T. P.; Logan, J. A.; Kikuchi, H.; Sands, J. M.; Kumar, S. K. Near-surface alignment of polymers in rubbed films. *Nature* **1995**, *374*, 709–711.

35 Dante, M.; Peet, J.; Nguyen, T. Q. Nanoscale charge transport and internal structure of bulk heterojunction conjugated polymer/fullerene solar cells by scanning probe microscopy. *J. Phys. Chem. C* **2008**, *112*, 7241–7249.

36 Barbara, P. F.; Adams, D. M.; O'Connor, D. B. Characterization of organic thin film materials with near-field scanning optical microscopy (NSOM). *Annu. Rev. Mater. Sci.* **1999**, *29*, 433–469.

37 Chiesa, M.; Burgi, L.; Kim, J.; Shikler, R.; Friend, R.; Sirringhaus, H. Correlation between surface photovoltage and blend morphology in polyfluorene-based photodiodes. *Nano Lett.* **2005**, *5*, 559–563.

38 Pingree, L. S. C.; Reid, O. G.; Ginger, D. S. Electrical scanning probe microscopy on active organic electronic devices. *Adv. Mater.* **2009**, *21*, 19–28, and references cited therein.

39 Reid, O. G.; Munechika, K.; Ginger, D. S. Space charge limited current measurements on conjugated polymer films using conductive atomic force microscopy. *Nano Lett.* **2008**, *8*, 1602–1609.

40 Coffey, D. C.; Reid, O. G.; Rodovsky, D. B.; Bartholomew, G. P.; Ginger, D. S. Mapping local photocurrents in polymer/fullerene solar cells with photoconductive atomic force microscopy. *Nano Lett.* **2007**, *7*, 738–744.

41 Yu, G.; Gao, J.; Hummelen, J. C.; Wudl, F.; Heeger, A. J. Polymer photovoltaic cells - enhanced efficiencies via a network of internal donor-acceptor heterojunctions. *Science* **1995**, *270*, 1789–1791.

42 Halls, J. J. M.; Walsh, C. A.; Greenham, N. C.; Marseglia, E. A.; Friend, R. H.; Moratti, S. C.; Holmes, A. B. Efficient photodiodes from interpenetrating polymer networks. *Nature* **1995**, *376*, 498–500.

43 Shaheen, S. E.; Brabec, C. J.; Sariciftci, N. S.; Padinger, F.; Fromherz, T.; Hummelen, J. C. 2.5% efficient organic plastic solar cells. *Appl. Phys. Lett.* **2001**, *78*, 841–843.

44 Park, S. H.; Roy, A.; Beaupre, S.; Cho, S.; Coates, N.; Moon, J. S.; Moses, D.; Leclerc, M.; Lee, K.; Heeger, A. J. Bulk heterojunction solar cells with internal quantum efficiency approaching 100%. *Nat. Photon.* **2009**, *3*, 297–302.

45 Reyes-Reyes, M.; Kim, K.; Carroll, D. L. High-efficiency photovoltaic devices based on annealed poly(3-hexylthiophene) and 1-(3-methoxycarbonyl)-propyl-1-phenyl-(6,6)C-61 blends. *Appl. Phys. Lett.* **2005**, *87*, 083506.

46 Chirvase, D.; Parisi, J.; Hummelen, J. C.; Dyakonov, V. Influence of nanomorphology on the photovoltaic action of polymer-fullerene composites. *Nanotechnology* **2004**, *15*, 1317–1323.

47 Al-Ibrahim, M.; Ambacher, O.; Sensfuss, S.; Gobsch, G. Effects of solvent and annealing on the improved performance of solar cells based on poly(3-hexylthiophene): Fullerene. *Appl. Phys. Lett.* **2005**, *86*, 201120.

48 Groves, C.; Koster, L. J. A.; Greenham, N. C. The effect of morphology upon mobility: Implications for bulk heterojunction solar cells with nonuniform blend morphology. *J. Appl. Phys.* **2009**, *105*, 094510.

49 Watkins, P. K.; Walker, A. B.; Verschoor, G. L. B. Dynamical Monte Carlo modelling of organic solar cells: The dependence of internal quantum efficiency on morphology. *Nano Lett.* **2005**, *5*, 1814–1818.

50 Cadby, A.; Khalil, G.; Fox, A. M.; Lidzey, D. G. Mapping exciton quenching in photovoltaic-applicable polymer blends using time-resolved scanning near-field optical microscopy. *J. Appl. Phys.* **2008**, *103*, 093715.

51 Marsh, R. A.; Groves, C.; Greenham, N. C. A microscopic model for the behavior of nanostructured organic photovoltaic devices. *J. Appl. Phys.* **2007**, *101*, 083509.

52 Rappaport, N.; Bar, Y.; Solomeshch, O.; Tessler, N. Mobility spatial distribution function: Comparative method for conjugated polymers/molecules. *Appl. Phys. Lett.* **2006**, *89*, 252117.